Turkish Journal of Electrical Engineering & Computer Sciences

http://journals.tubitak.gov.tr/elektrik/

Research Article

Turk J Elec Eng & Comp Sci
(2017) 25: 2922 – 2932

doi:10.3906/elk-1605-6

A spectral element method for the solution of magnetostatic fields

Ibrahim MAHARIQ[1,2,*], **Atakan ERCIYAS**[2]

[1]Department of Electrical and Electronics Engineering, TOBB University of Economics and Technology, Ankara, Turkey

[2]Electrical & Electronics Engineering, Faculty of Engineering, University of Turkish Aeronautical Association, Ankara, Turkey

Received: 02.05.2016 • **Accepted/Published Online:** 11.11.2016 • **Final Version:** 30.07.2017

Abstract: Recently, we have seen good progress in our capability to simulate complex electromagnetic systems. However, still there exist many challenges that have to be tackled in order to push limits restricting the field of computational electromagnetics upward. One of these challenges is the limitations in the available computational resources. Over several decades, the traditional computational methods, such as finite difference, finite element, and finite volume methods, have been extensively applied in the field of electromagnetics. On the other hand, the spectral element method (SEM) has been recently utilized in some branches of electromagnetics as waveguides and photonic structures for the sake of accuracy. In this paper, the numerical approximation to the set of the partial differential equations governing a typical magnetostatic problem is presented by using SEM for the first time to the best of our knowledge. Legendre polynomials and Gauss–Legendre–Lobatto grids are employed in the current study as test functions and meshing of the elements, respectively. We also simulate a magnetostatic problem in order to verify the SEM formulation adapted in the current study.

Key words: Computational electromagnetics, finite element method, magnetostatics, spectral element method

1. Introduction

Electromagnetic problems are typically defined by Maxwell equations that describe to us how electric and magnetic fields are generated and their effects on each other. However, it is quite difficult to solve them by analytical methods owing to their being part of partial differential equations [1]. Fortunately, there are some numerical methods in which Maxwell's equations are approximated to obtain the associated solutions with acceptable accuracies, thanks to computational electromagnetics developed in parallel with improvement in computing machines.

Numerical methods are discriminated among each other mainly according to some key points such as accuracy and requirements of computational resources (available CPU and memory). That is, a numerical method may have less computational time than another as it has more memory consumption, or vice versa [2–4]. Among these numerical methods that have been being applied intensively for several decades are the finite difference method (FDM) and the finite element method (FEM).

FEM is one of the most powerful numerical methods ever invented to solve partial differential and integral equations of initial and boundary-value problems (BVPs) in complex geometries. In the early 1960s engineers

*Correspondence: ibmahariq@gmail.com

used the method in order to approximate the solution in different research areas such as fluid dynamics and heat transfer. In the late 1960s and early 1970s it began to be applied in engineering problems. Continuous quantities such as pressure and temperature can be modeled by discrete finite elements as polynomials.

The FDM is another approach to solve Maxwell's equations. In order to apply this method, first the problem domain should be discretized, and the discretization process is done by dividing the problem domain into equispaced elements. This method has two computational error sources: round-off error and truncation error. Round-off error is based on loss of precision of decimal quantities owing to iterations on computing process. The truncation error, also known as discretization error, consists of samples taken from each step in computation to approximate infinite elements [5].

Many studies have been introduced in the literature over the past decades calculating magnetic fields associated with low-frequency magnetic problems. Most of the recent work has been devoted to studying minor details such as boundary conditions, numerical iterations, and little improvements in accuracy. For instance, Biro [6] utilized various FEM techniques on three-dimensional magnetostatic problems in order to improve numerical stability.

In [7], a novel analytical solution of the airgap region is derived and coupled with the FEM equations in order to solve the field in an electrical machine for both rotor and stator regions. The motivation behind that study was to naturally couple the analytical solution with the FEM equations based on the continuity of magnetic vector potentials across their boundaries. Consequently, the stiffness matrix was derived. Results and experiments show that computational time is approximately the same due to analytical computation despite the fact that it is expected to have fewer nodes in finite elements.

The spectral element method (SEM), on the other hand, was first introduced by Patera [8] in 1984 for computational fluid dynamics. Patera proposed a SEM that combines the flexibility of the FEM with the accuracy of spectral methods.

Generally speaking, spectral element methods are considered a family of approximation schemes based on the Galerkin method. They share common characteristics with finite-element discretizations, and this provides the reason why they can be viewed as h- or p-versions of the FEM. That is, when viewed as h-version, a Lagrangian interpolation formula on the parent element exists in both, and the basis functions have local support. On the other hand, SEMs use high-degree polynomials on a fixed geometric mesh for the sake of enhanced accuracy, and this is the fact characterizing the p-version of FEMs [9].

In the recent literature, some details regarding the application of the SEM in electromagnetic wave propagation have been investigated. In Sjögren et al. [10], the comparison of FDM and SEM over material discontinuity is studied. It is stated that the FDM and SEM can simulate simple cases of wave reflection and refraction in two-dimensional rectangular geometry accurately. For a particular geometry, the FDM is better suited and has higher efficiency. However, in more complicated geometries, the SEM has more advantages due to the fact that it is easier to implement an unstructured grid. Besides that, this method also suited well for parallel implementations for large computations. Similar results were confirmed by Airiau [11] and Christoph [12] in which the discontinuous Galerkin spectral element method is considered.

To the best of our knowledge, when the literature is searched, one can observe that SEM has not been applied in magnetostatic or quasi-magnetostatic problems. It is noteworthy to mention that spectral methods (but not the SEM) were introduced in 1983 by Steele [13]. The author utilized a spectral method in which the magnetic fields are computed by expressing them as a linear combination of a set of orthogonal functions. The only advantage pointed out by the author is the reduction in the size of the system of linear equations when

compared with the FEM. However, spectral methods are not successful in solving domains involving complex geometries and/or nonhomogeneous materials. For that reason, people later on did not extend Steele's work.

In this paper, the SEM is applied in modelling of time-invariant, two-dimensional magnetostatic problems. The reduced computational cost and the accuracy offered by SEM are the main motivation behind the present study [2–4,14,15]. As most magnetostatic problems are complex in nature, the application of the SEM in low-frequency magnetic problems forms a new spot towards improving the accuracy of designs performed by engineers and specialists.

The paper is arranged as follows: section 2 reviews the derivations of the governing partial differential equations in magnetostatics. In section 3, the spatial approximation to these equations is presented by SEM. A typical demonstration is discussed and presented in section 4, and finally some conclusions and future works associated with the interest of this paper are introduced in the last section.

2. Problem formulation

Magnetostatic problems are a special case of electromagnetic problems. In a magnetostatic problem, where only magnetic fields in a given structure are solved, the currents are steady or said to be time-invariant.

Gauss's law for magnetism and Ampere's law are expressed respectively in differential form as

$$\nabla \cdot \overrightarrow{B} = 0 \tag{1}$$

$$\nabla \times \overrightarrow{H} = \overrightarrow{J}, \tag{2}$$

in which $\overrightarrow{J}$ stands for the injected current density, $\overrightarrow{B}$ is the vector field of the magnetic flux density, and $\overrightarrow{H}$ is the field intensity, and are related as $\overrightarrow{B} = \mu \overrightarrow{H}$, with μ being the magnetic permeability. Due to Helmholtz decomposition theorem, the magnetic flux density has a unique potential vector, $\overrightarrow{A}$, such that

$$\overrightarrow{B} = \nabla \times \overrightarrow{A} \tag{3}$$

By substituting Eq. (3) in (2), the following differential equation is obtained:

$$\nabla \times \left(\frac{1}{\mu} \nabla \times \overrightarrow{A} \right) = \overrightarrow{J} \tag{4}$$

Since the magnetic material is assumed to be homogeneous, μ can be out of differentiation, and one can rewrite Eq. (4) as

$$\nabla \left(\nabla \cdot \overrightarrow{A} \right) - \nabla^2 \overrightarrow{A} = \mu \overrightarrow{J} \tag{5}$$

in which ∇^2 stands for the vector Laplacian. With the choice of the gauge

$$\nabla \cdot \overrightarrow{A} = 0 \tag{6}$$

Eq. (5) leads to the Poisson equation

$$\nabla^2 \overrightarrow{A} = -\mu \overrightarrow{J} \tag{7}$$

In two-dimensional Cartesian coordinates (2D), if $\overrightarrow{J} = J_z(x,y)\hat{a}_x$, then $\overrightarrow{A} = A_z(x,y)\hat{a}_z$, meaning that the solution is sought for the z-component only, i.e. let the scalars A, J be $A = A_z(x,y)$ and $J = J_z(x,y)$. Therefore, Eq. (7) reads as

$$\frac{\partial^2 A}{\partial x^2} + \frac{\partial^2 A}{\partial y^2} = -\mu J \tag{8}$$

and it must be satisfied in magnetic materials where currents flow, with the following equations:

$$\frac{\partial^2 A}{\partial x^2} + \frac{\partial^2 A}{\partial y^2} = -\mu_0 J \tag{9}$$

$$\frac{\partial^2 A}{\partial x^2} + \frac{\partial^2 A}{\partial y^2} = 0 \tag{10}$$

in a coil region and in air, respectively.

The application of boundary conditions is important in order to provide unique solution of the partial differential equations. In magnetic and electrostatic problems, there are some boundary conditions that are commonly used [16]. The Dirichlet boundary condition defines the value of potential explicitly on the boundary. In fact, in most of magnetic problems, the zero Dirichlet condition is introduced.

However, in the Neumann boundary condition, the normal derivative of potential along the boundary is defined. In magnetic problems, the derivative of magnetic potential is set to zero along the boundary so that magnetic flux is forced to pass the boundary at 90° angle [16].

There is another boundary condition called the Robin boundary condition that combines the Dirichlet and Neumann boundary conditions. It describes the value of vector potential and its normal derivative at the boundary. In periodic boundary conditions, two boundaries are joined together.

3. SEM formulation

Patera [8] offered a spectral element method that utilizes the flexibility of the FEM and the accuracy of the spectral method. There are mainly two techniques that are utilized in the SEM. One depends on Chebyshev polynomials and the other is based on Legendre polynomials. Both implementations employ Gauss–Legendre–Lobatto (GLL) quadrature grids in order to achieve Langrangian interpolation.

In the current study, we apply the SEM based on Legendre polynomials as test functions, and GLL quadrature grids in order to perform Lagrangian interpolation [8,9,17].

We seek an approximate solution to the presented set of partial differential equations in the trial space

$$A = \left\{ A_z \in H \;\middle|\; A_z|_{\partial\Omega_D} = f_{bc}, \quad \tfrac{\partial}{\partial n} A_z\big|_{\partial\Omega_N} = g \right\} \tag{11}$$

The residual resulting from the substitution of the approximate solution from the trial space into Eqs. (8)–(10) is then projected onto the test space:

$$V = \{ v \in H |\; v|_{\partial\Omega_D} = 0 \} \tag{12}$$

The projection is performed by using the weighted inner product operation:

$$(v, A_z)_\omega \equiv \int_\Omega \omega\, \bar{v}\, A_z d\mathbf{x} \tag{13}$$

in the Hilbert space H, where the overbar denotes complex conjugation. The projection procedure

$$(v, \nabla^2 A_z - \mu J_z)_\omega = 0 \tag{14}$$

and the variational (weak) form is obtained as (after integration by parts)

$$\int_\Omega \nabla(\omega\,\bar{v}) \cdot \nabla A_z\, dx - \mu J_z \int_\Omega \omega\,\bar{v}\; dx = \int_{\partial\Omega_N} \omega\,\bar{v}\; g\, dx \tag{15}$$

Adapting the formulation to arbitrary domain geometry is achieved in two steps. The first involves partitioning of the domain into M-mutually disjoint elements:

$$\Omega = \Omega^1 \cup ... \cup \Omega^e ... \cup \Omega^M = \bigcup_{e=1}^{M} \Omega^e. \tag{16}$$

A typical integral in the variational form then becomes

$$\int_\Omega \omega\,\bar{v}\; A_z\, d\mathbf{x} = \sum_{e=1}^{M} \int_{\Omega^e} \omega\,\bar{v}\; A_z\, d\mathbf{x}, \tag{17}$$

The second step is to introduce the standard square element

$$\Omega^{std} = \left\{(\xi,\eta) \in \Re^2 \;\mid\; -1 \le \xi \le 1,\; -1 \le \eta \le 1\right\} \tag{18}$$

that will standardize and facilitate the integral operations over a general quadrilateral element Ω^e through mapping:

$$x = \chi_1^e(\xi,\eta), \quad y = \chi_2^e(\xi,\eta). \tag{19}$$

The operations can then be converted using the rules:

$$\begin{bmatrix} dx \\ dy \end{bmatrix} = \underbrace{\begin{bmatrix} \frac{\partial \chi_1^e}{\partial \xi} & \frac{\partial \chi_1^e}{\partial \eta} \\ \frac{\partial \chi_2^e}{\partial \xi} & \frac{\partial \chi_2^e}{\partial \eta} \end{bmatrix}}_{\mathbf{J}} \begin{bmatrix} d\xi \\ d\eta \end{bmatrix} \tag{20}$$

$$\nabla = \begin{bmatrix} \frac{\partial}{\partial x} \\ \frac{\partial}{\partial y} \end{bmatrix} = \frac{1}{|\mathbf{J}|} \begin{bmatrix} \frac{\partial \chi_2^e}{\partial \eta} & -\frac{\partial \chi_1^e}{\partial \eta} \\ -\frac{\partial \chi_2^e}{\partial \xi} & \frac{\partial \chi_1^e}{\partial \xi} \end{bmatrix} \begin{bmatrix} \frac{\partial}{\partial \xi} \\ \frac{\partial}{\partial \eta} \end{bmatrix}, \tag{21}$$

where $|J|$ is the determinant of the Jacobian.

The associated roots ς_m as nodes provide the stable form of interpolation

$$A_z(\varsigma) = \sum_{m=0}^{N} A_z(\varsigma_m) L_m(\varsigma), \tag{22}$$

where L denotes respective Lagrange interpolants with the typical form

$$L_k(\varsigma) = \prod_{\substack{\ell = 0 \\ \ell \neq k}}^{N} \frac{(\varsigma - \varsigma_\ell)}{(\varsigma_k - \varsigma_\ell)} \tag{23}$$

satisfying the cardinality property $L_k(\varsigma_\ell) = \delta_{k\ell}$. This provides the means for evaluating the derivatives,

$$\frac{d}{d\varsigma} A_z(\varsigma)\big|_{\varsigma_k} = \sum_{m=0}^{N} A_z(\varsigma_m) L'_m(\varsigma_k) = \sum_{m=0}^{N} A_z(\varsigma_m) \underbrace{L'_m(\varsigma_k)}_{D_{km}}, \tag{24}$$

where D_{km} stands for the differentiation matrix. It also provides GLL quadrature

$$\int_{-1}^{1} A_z(\varsigma)\, d\varsigma = \sum_{k=0}^{N} \varpi_k A_z(\varsigma_k) \tag{25}$$

These can easily be extended to two dimensions over the tensor grid (ξ_k, η_ℓ) with the mapping functions $\chi_i(\xi, \eta)$ constructed by using the linear blending function approach [9,18]. It is noteworthy to mention that MATLAB was utilized in the numerical implementation of the SEM formulation.

It is more an art experience than a science to know how to optimally place and size the mesh in the FEM. In fact, experience taught us to have more elements in the physical domain where functions change rapidly and have fewer elements where low gradients are expected. Mesh generation may take several trials before a good mesh distribution is achieved. On the other hand, the complexity in the physical domain itself may add additional limitations to mesh generation [19].

In contrast, the SEM has the flexibility of using a larger elemental aspect ratio without significant deterioration in accuracy. For instance, Dong et al. [20] proposed a parallel SEM for dynamic three-dimensional nonlinear elasticity problems that provides a tolerant large elemental aspect ratio employing Jacobi polynomial-based shape functions, as an alternative to the typical Legendre polynomial-based shape functions in solid mechanics. Gwynllyw et al. [21] proposed an iterative method for moving SEM applied to the journal bearing problem where they investigated the results of an extremely large physical aspect ratio. In conclusion, the basis behind the mesh optimality in the case of the SEM differs from that of the FEM case. However, since this topic is an important aspect and as it does not lie within the scope of the current study, the authors will discuss and investigate mesh optimality by SEM in a future work because of the limitation on paper length.

4. Simulation results

In order to verify the formulation of the spectral element method adapted in the current study, a typical magnetic problem is considered in time-invariant domain. The structure is composed of a steel core having two windows as shown in Figure 1. A coil is placed on the middle leg and carries the electric current. The dimensions of the structure are chosen so that the magnetic flux flowing in the middle leg is shared equally between the left leg and right leg.

As the problem is unbounded in nature, one needs to truncate it so that it becomes computationally feasible. For this purpose, we assigned the Dirichlet boundary condition ($A = 0$) on the exterior boundary,

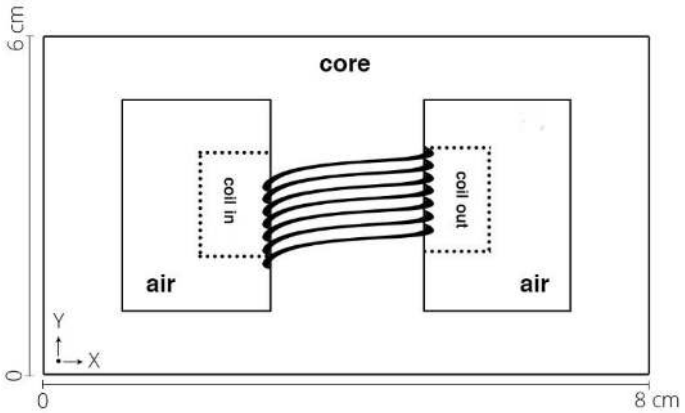

Figure 1. The structure of the simulated problem.

which is placed at a distance equals to twice of the width of an outer leg. In fact choosing $A = 0$ will not affect the solution as the magnetic flux density is calculated based on the change in the vector potential as

$$B_x = \frac{\partial A}{\partial y}, \text{ and } B_y = \frac{\partial A}{\partial x}. \tag{26}$$

The governing differential equations to be satisfied in each region are derived and stated in Section 2. However, in order to solve it, the problem requires interface conditions that must hold between adjacent regions (as air-core interference). This condition is satisfied by specifying the value of the normal component of

$$\hat{n}.(\frac{1}{\mu}\nabla A) \tag{27}$$

on the boundary. This is equivalent to specifying the tangential value of the magnetic field intensity on the boundary.

The computational domain as pointed out earlier in this study has to be discretized into elements. Figure 2 shows the elements composing the computational domain and the GLL grids in each element. In this figure, the dark gray region represents the core, whereas the coil is represented by light gray regions. As can be seen from the figure, meshing in the SEM is similar to that of the FEM. In other words, the elements are getting larger and larger as we move away from the critical regions. In Figure 3, we share the solution of the vector magnetic potential in the domain. The corresponding injected current is $10\,A/mm^2$ and at a core relative magnetic permeability of 2000 H/m. The associated contour plot is shown in Figure 4. As can be clearly seen from the figure, flux density in the air is almost zero. This is because of the relatively high magnetic permeability defining the steel.

It is worthy to note that since our problem is symmetrical around the x-axis, the computational domain is reduced to half. To account for this symmetry, the Neumann boundary condition has to be applied, i.e.

$$\frac{\partial A}{\partial y} = 0 \tag{28}$$

In this work, the continuous Galerkin method is adapted. This means that nodes that lie on the boundaries of an element must be same as those corresponding to adjacent elements. On the other hand, one can use the

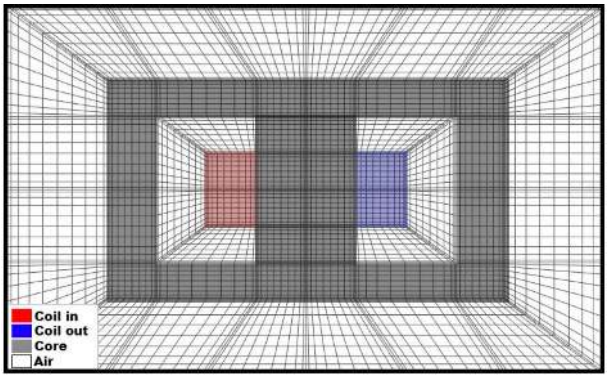

Figure 2. Gauss–Legendre–Lobatto grids in the elements forming the computational domain.

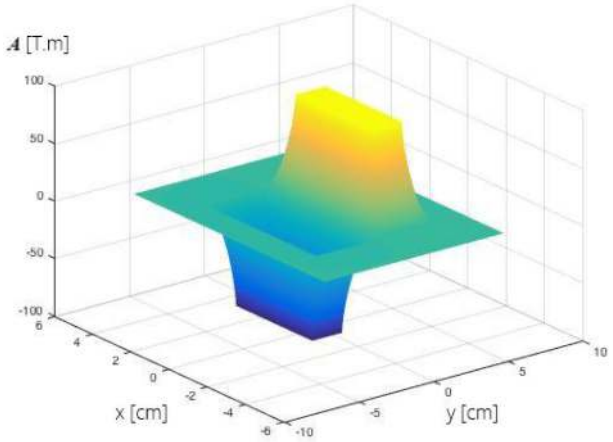

Figure 3. The solution of the vector magnetic potential.

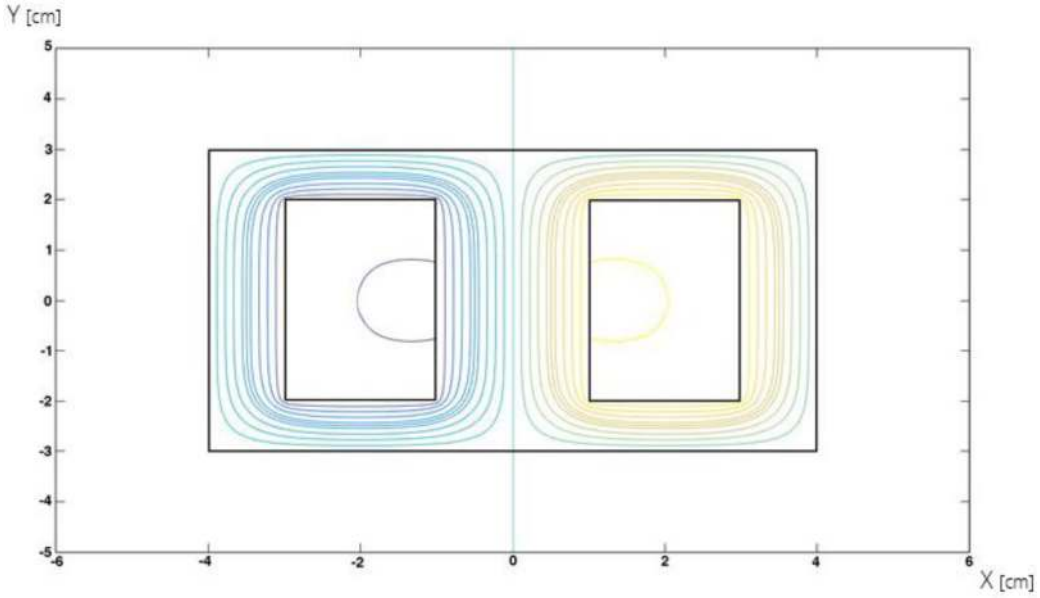

Figure 4. The contour plot of the vector magnetic potential.

discontinuous Galerkin method; in this case Riemann solvers must be utilized in order to match the solution at the interfaces between elements [22].

For the purpose of comparison, the same structure introduced in Figure 1 is solved by FEM as shown in Figure 5, in which triangular elements are used to discretize the computational domain. The contours of the magnetic vector potential are also presented on the same figure. Figure 6 presents the magnetic field density (B) as obtained by SEM and FEM across the points forming the line ab shown in Figure 5. The average of B is about 35.4 Tesla. As can be seen from Figure 6, SEM shows smoother variation in B and symmetric around x = 0. The maximum difference between the SEM and FEM results is around 1.12%. However, although this is acceptable in terms of the engineering point of view, one should not forget the other advantages of SEM from the view of computational aspects. Triangular elements can be utilized by SEM as investigated by [23], but since it adds more complexity to numerical implementation, our study is based on the application of quadrilateral

elements with straight or curved sides as GLL is considered for nodal distribution. Some examples of these quadrilateral elements are shown in Figure 7. This flexibility in the shapes of SEM elements can be utilized in meshing complex geometries where different scattering objects of arbitrary shapes are involved. Finally, we show in Figure 8 a typical GLL nodes distribution in a curved sided quadrilateral element that can also be utilized by SEM.

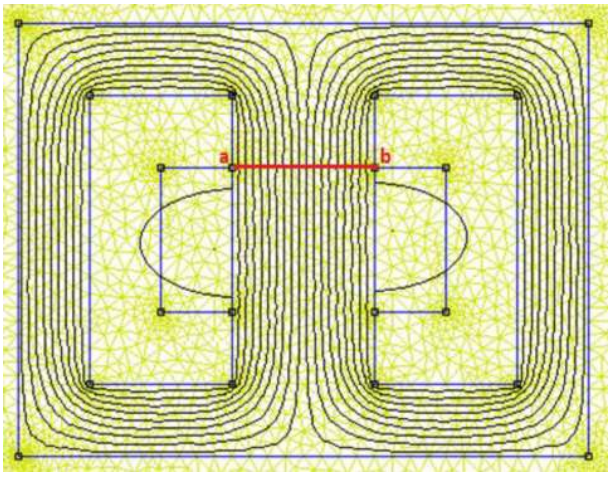

Figure 5. Meshing and contour plots by FEM.

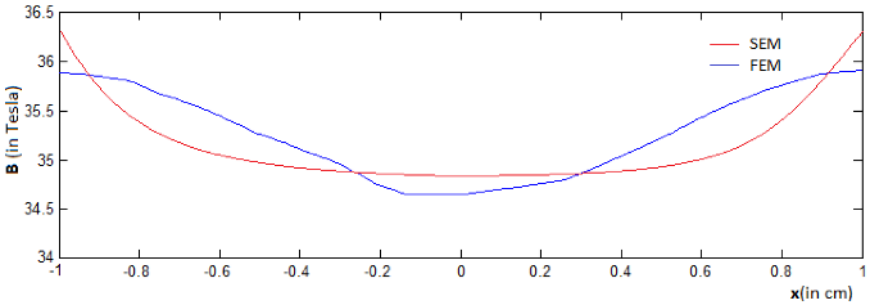

Figure 6. SEM and FEM magnetic flux densities across the line ab (shown in Figure 5).

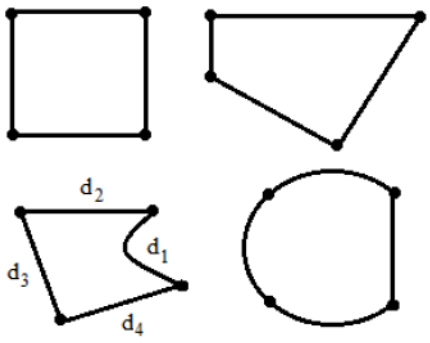

Figure 7. Various quadrilateral elements can be utilized by SEM.

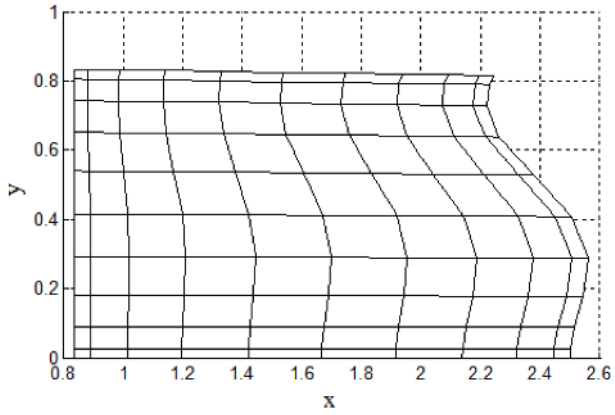

Figure 8. Distribution of GLL nodes in a curved sided quadrilateral element.

Based on the formulation presented in the current study, the resulting system after discretized by SEM is complex valued. In other words, both the real part and the imaginary part of the unknowns must be solved. This system is linear, sparse, symmetric, indefinite, and relatively ill-conditioned. Hence, solving this system requires an iterative method, and to efficiently solve it, a suitable preconditioner must be applied. Conjugate gradient (CG) method or the generalized minimum residual (GMRES) method can be utilized with Jacobi, ILU decomposition, or successive over relaxation as a preconditioner.

5. Conclusion

In this study, we have presented, for the first time, the formulation of a typical magnetostatic problem by the SEM. In addition, we have provided to the reader a typical simulation example showing the successful application of the method. Although the adapted formulation is based on the continuous Galerkin approach, it is also possible to utilize the discontinuous approach.

As pointed out throughout the paper, the SEM offers higher accuracy than the traditionally applied FEM. Moreover, it has less computational cost. The latter advantage is very valuable when dealing with large computational problems that cannot be performed sometimes because of limited available memory.

References

[1] Umashankar K, Allen T. Computational Electromagnetics. Norwood, MA, USA: Artech House on Demand, 1993.

[2] Lee J, Xiao T, Liu QH. A 3-D spectral-element method using mixed-order curl conforming vector basis functions for electromagnetic fields. IEEE T Microw Theory 2006; 54: 437-444.

[3] Lee J, Liu QH. A 3-D spectral-element time-domain method for electromagnetic simulation. IEEE T Microw Theory 2007; 55: 983-991.

[4] Mahariq I, Kurt H, Kuzuoğlu M. Questioning degree of accuracy offered by the spectral element method in computational electromagnetics. Appl Comput Electrom 2015; 30: 698-705.

[5] Causon DM, Mingham CG. Introductory Finite Difference Methods for PDEs. Frederiksberg, Denmark: Ventus Publishing Aps, 2010.

[6] Biro O, Preis K, Richter KR. On the use of the magnetic vector potential in the nodal and edge finite element analysis of 3D magnetostatic problems. IEEE T Magn; 1996: 32: 651-654.

[7] Chau K, Jiang J, Zhang D. A finite element-analytical method for electromagnetic field analysis of electric machines with free rotation. In: IEEE 2006 International Magnetics Conference; 8–12 May 2006; San Diego, CA, USA: IEEE. pp. 495-496.

[8] Patera AT. A spectral element method for fluid dynamics: laminar flow in a channel expansion. J Comput Phys 1984; 54: 468-488.

[9] Deville MO, Fischer PF, Mund EH. High-Order Methods for Incompressible Fluid Flow. Cambridge, UK: Cambridge University Press, 2002.

[10] Sjögren M. Comparison of spectral element and finite difference methods for electromagnetic wave propagation over a material discontinuity. Swedish Defence Research Agency Stockholm. FOI-R–0489—SE. Sci. Rep. 2002.

[11] Airiau S, Azaïez M, Belgacem FB, Guivarch R. Parallelization of spectral element methods. In: High Performance Computing for Computational Science – VECPAR; 26–28 June 2002; Porto, Portugal: Lect Notes Comput Sc. pp. 392-403.

[12] Keller R, Kramer D, Weiss JP. Facing the Multicore-Challenge III. Berlin, Germany: Springer, 2013.

[13] Steele CW. A spectral method for field computation. IEEE T Magn 1983; 19: 2296-2299.

[14] Mehdizadeh OZ, Paraschivoiu M. Investigation of a two-dimensional spectral element method for Helmholtz's equation. J Comput Phys 2003; 189: 111-129.

[15] Mahariq I, Kurt H, Tarman H, Kuzuoğlu M. Photonic nanojet analysis by spectral element method. IEEE Phot J 2014; 6: 1-14.

[16] Dede E, Ercan M, Jaewook L, Nomura T. Multiphysics Simulation: Electromechanical System Applications and Optimization. London, UK: Springer, 2014.

[17] Karniadakis G, Sherwin S. Spectral/hp Element Methods for Computational Fluid Dynamics. Oxford, UK: Oxford University Press, 2007.

[18] Gordon JW, Hall AC. Transfinite element methods: blending-function interpolation over arbitrary curved element domains. Numerische Mathematik 1973; 21: 109-129.

[19] Pepper DW, Heinrich JC. Finite Element Methods: Basic Concepts and Applications. 1st ed. Boca Raton, FL, USA: CRC Press, 1992.

[20] Dong S, Yosibash Z. A parallel spectral element method for dynamic three-dimensional nonlinear elasticity problems. Comput Struct 2012; 87: 59-72.

[21] Gwynllyw DR, Phillips TN. Iterative methods with dynamic preconditioning for moving spectral element technique applied to the journal bearing problem. In: Proceedings of the Third International Conference on Spectral and High Order Methods; 5–9 June 1995; Houston, TX, USA: Houston J Math. pp. 277-286.

[22] Lee J, Chen J, Liu Q. A 3-D discontinuous spectral element time-domain method for Maxwell's equations. IEEE T Antenn Propag 2009; 57: 2666-2674.

[23] Sherwin SJ, Karniadakis GE. A triangular spectral element method; applications to the incompressible Navier-Stokes equations. Comput Method Appl M 1995; 123: 189-229.